Loss Reduction in V/f Control for Switched Reluctance Motor Driven by Single-Pulse Voltage

Hirotaka Kato*, Hiroki Watanabe*, and Jun-ichi Itoh*
* Nagaoka University of Technology,
1603-1, Kamitomioka-machi, Nagaoka-shi, Niigata, 940-2188, Japan

***Abstract*-- This paper proposes a single-pulse drive method in V/f control, which consists of two original approaches and one modification: (i) generation of a single-pulse voltage with a zero-voltage period, (ii) correction method for a conduction period error due to a discrete control system, and (iii) modification of the high-efficiency control to specialize in single-pulse voltage drive. The proposed method reduces of 11.7% of the copper loss and 19.2% of the iron loss in the experiment.**

***Index Terms*— Loss reduction, Single-pulse voltage, Switched reluctance motor, V/f control.**

I. Introduction

Switched reluctance motors (SRMs) consist only of iron cores and windings without permanent magnets using rare earth elements, which are inexpensive to manufacture. SRMs have attracted attention as adjustable-speed motors for industrial applications due to the robust salient pole structures of their rotor [1-3]. Adjustable-speed drive systems without position sensors are expected for SRMs to take advantage of high-temperature and high-speed durability and cost-effectiveness.

Many studies have been conducted on the rotor position sensorless control methods with the estimated position using the position dependency of inductance [4-7]. In these methods, the instantaneous value of the inductance is first calculated from the voltage and current. Then, the calculated inductance is converted into the rotor position information with a look-up table or an approximation formula of the relationship between inductance and rotor position. However, these methods require complicated control algorithms such as harmonic voltage superposition [4][5] or additional analog circuits [6][7] to detect the instantaneous inductance accurately. In addition, there is concern about the effect of position estimation errors in the high-speed operation range [8]. The authors have proposed the V/f control for SRMs [9], which does not require rotor position information due to its control strategy based on the rotating coordinate system relative to the converter output voltage. Thus, the V/f control does not have the problem of the inductance detection accuracy and conversion accuracy to the rotor position.

The V/f control of SRMs uses the mathematical model shown in Ref. [10] to achieve the simple control. The mathematical model approximates the inductance distribution of the SRM with the sinusoidal waveform. However, the actual model of the SRM contains many spatial harmonics, in different from the mathematical model. As a result, the maximum torque per ampere (MTPA) condition shown in Ref. [10] does not always minimize the motor loss.

On the other hand, single-pulse voltage drive methods with position sensors have been studied as highly efficient driving methods for SRMs [11-15]. These methods maximize the drive efficiency by minimizing the conduction period in the negative torque section. However, they require the optimization of three parameters: the turn-on-angle, zero-voltage-start-angle, and turn-off-angle. Ref. [11] proposes losses modeling method using only simple analytical results. However, control system design is complicated because parameters must be adjusted by trial and error at all operating points.

This paper proposes a loss reduction method based on the V/f control of SRMs driven by single-pulse voltage. The proposed method achieves both simple designs and high-efficiency drives by applying the single-pulse voltage to the V/f control using the mathematical model. The single-pulse voltage is generated so that the fundamental component matches the command value of the V/f control. Thus, it is uniquely determined without the need for complicated adjustments. The control configuration is based on the V/f control of SRMs proposed in Ref. [9] with the following modifications: (i) generation of the single-pulse voltage, (ii) correction of the conduction period error in the discrete control system, and (iii) modification of the high-efficiency control specialized for the single-pulse voltage drive. The proposed method achieves the V/f control with the single-pulse voltage, which suppresses the motor current beat. The copper loss is reduced by 11.7% and iron loss by 19.2% compared with that of the conventional sinusoidal voltage drive from the experimental verification.

II. PROPOSED SINGLE-PULSE DRIVE METHOD

Fig. 1 shows the control block diagram of the V/f control of the SRM. The V/f control consists of the zero-phase current control, the V/f control including the damping control, and the high-efficiency control. In this paper, the proposed method reduces the motor loss by two original approaches and one modification, generating the single-pulse voltage, correcting the conduction period error, and modifying of the high-efficiency control specialized for single-pulse drive.

A. Generation of single-pulse voltage

Fig. 2 shows the proposed single-pulse voltage waveform. The proposed waveform shown in Fig. 2 (b) reduces the conduction period in the negative torque section by using the pulse-voltage to quickly flow and pull out the motor current compared to the sinusoidal voltage drive shown in Fig. 2 (a). Three parameters are used to generate the single-pulse voltage: turn-on angle θ_{on}, zero-volt-loop period $\Delta\theta_{\mathrm{ZVL}}$, and turn-off-angle θ_{off}. The fundamental component $v_{\mathrm{fnd.}}$ and the zero-phase component v_{zero} of the single-pulse voltage are expressed as in (1),

$$\begin{cases} v_{\mathrm{fnd.}} = \sqrt{v_{a1}^2 + v_{b1}^2} \\ v_{\mathrm{zero}} = \dfrac{E_{\mathrm{dc}}}{2\pi}\left(2\pi - \theta_{\mathrm{on}} - \theta_{\mathrm{off}}\right) \end{cases} \tag{1}$$

where,

$$\begin{aligned} v_{a1} &= -\frac{E_{\mathrm{dc}}}{\pi}\left(\sin\theta_{\mathrm{on}} + \sin\theta_{\mathrm{off}}\right) \\ v_{b1} &= \frac{E_{\mathrm{dc}}}{\pi}\left\{2\cos\left(\Delta\theta_{\mathrm{ZVL}}/2\right) + \cos\theta_{\mathrm{on}} + \cos\theta_{\mathrm{off}}\right\} \end{aligned} \tag{2}$$

Note that E_{dc} is a DC link voltage of the converter. Assuming that $v_{\mathrm{fnd.}}$ is sufficiently large relative to v_{zero} in (1), θ_{on} and θ_{off} are expressed as in (3),

$$\begin{cases} \theta_{\mathrm{on}} = \arccos\left\{\dfrac{v_{\mathrm{fnd.}}}{2E_{\mathrm{dc}}}\pi - \cos\left(\Delta\theta_{\mathrm{ZVL}}/2\right)\right\} \\ \theta_{\mathrm{off}} = 2\pi - \theta_{\mathrm{on}} - \dfrac{2\pi v_{\mathrm{zero}}}{E_{\mathrm{dc}}} \end{cases} \tag{3}$$

Since $v_{\mathrm{fnd.}}$ and v_{zero} correspond to v_δ and v_0, respectively in V/f control, (4) is derived by substituting them into (3),

$$\begin{cases} \theta_{\mathrm{on}} = \arccos\left\{\dfrac{v_\delta}{2E_{\mathrm{dc}}}\pi - \cos\left(\Delta\theta_{\mathrm{ZVL}}/2\right)\right\} \\ \theta_{\mathrm{off}} = 2\pi - \theta_{\mathrm{on}} - \dfrac{2\pi v_0}{E_{\mathrm{dc}}} \end{cases} \tag{4}$$

The single pulse voltage is generated based on the voltage command of the V/f control. $\Delta\theta_{\mathrm{ZVL}}$ has a degree of freedom. Determining method of $\Delta\theta_{\mathrm{ZVL}}$ is described in Section C.

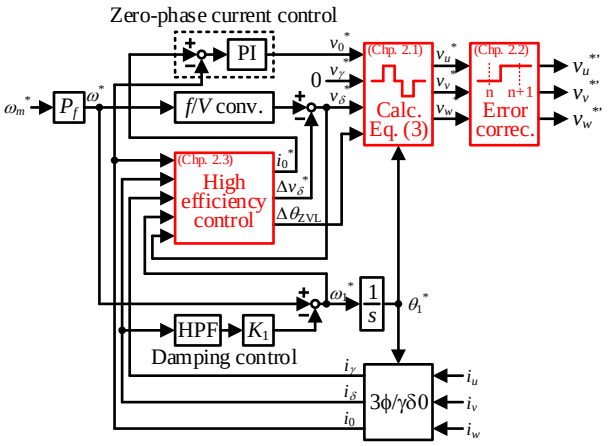

Fig. 1. Control diagram of proposed method.

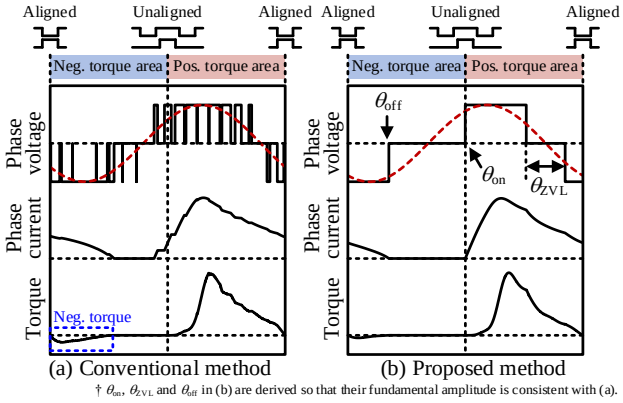

Fig. 2. Proposed drive waveform.

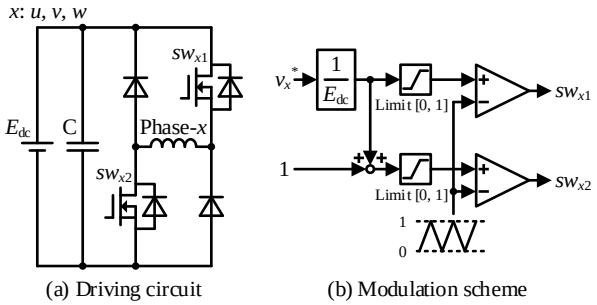

Fig. 3. Drive circuit and modulation scheme.

Fig. 3 shows the drive circuit and modulation scheme. The following operation modes are obtained when the unipolar modulation shown in Fig. 3 (b) is applied in an asymmetric half-bridge converter,

$$\begin{cases} sw_{x1} = sw_{x2} = 1, & (\text{when} \quad v_x^* = E_{\mathrm{dc}}) \\ sw_{x1} = 0, \quad sw_{x2} = 1 & (\text{when} \quad v_x^* = 0) \\ sw_{x1} = sw_{x2} = 0, & (\text{when} \quad v_x^* = -E_{\mathrm{dc}}) \end{cases} \tag{5},$$

where sw_{x1} and sw_{x2} are gate signals for the upper and lower sides of the converter, respectively, and v_x^* is the phase voltage command. The desired single-pulse voltage is generated by setting the voltage command to E_{dc} during the period from θ_{on} to the beginning of $\Delta\theta_{\mathrm{ZVL}}$, 0 during the

period of $\Delta\theta_{ZVL}$, and $-E_{dc}$ during the period from the end of $\Delta\theta_{ZVL}$ to θ_{off}. The proposed method is implemented using only a DSP without an FPGA because only the PWM is used to generate the gate signals.

B. Correction of conduction period error under PWM

Fig. 4 shows the effect of the conduction period error in the discrete system. The update timing of the gate signal in the controller depends on the calculation period in the case of the discrete control system. There is an error in the actual turn-on angle relative to the desired one. The conduction period error, which includes the beat of the current peak, causes the low-frequency noise and vibration shown in Fig. 4 (a). Especially in the high-speed range, the effect of the conduction period error cannot be ignored because the ratio of the calculation period to the fundamental period is large.

Fig. 5 shows the voltage command that corrects the conduction period error under the PWM. Assuming that the change in the armature inductance within the control period is small enough, the time integration of the applied voltage at the desired turn-on angle has to match that is modulated by the PWM. Thus, the voltage command v_u^* is corrected using (6) so that the area of the blue shaded line in Fig. 5 is equal for both.

$$v_u^* = \left(1 - \frac{\theta_{on} - \theta_{1\_n}}{\omega_1^* T_s}\right) \cdot E_{dc} \qquad (6),$$

where θ_{1_n} is the electric angle θ_1 calculated at period n inside the controller. This method increases the number of switching but suppresses the current conduction period error shown in Fig. 4 (b). $\Delta\theta_{ZVL}$ and θ_{off} are corrected in the same way.

C. High-efficiency control specialized for single-pulse voltage drive

Fig. 6 shows the block diagram of the high-efficiency control. The creative points from the high-efficiency control in V/f control for SRMs in Ref. [9] are the control method of the zero-phase current and θ_{ZVL}.

First, the generation method of zero-phase current command is explained. θ_{off} is determined by the output of the PI regulator expressed in (1). On the other hand, it is necessary to adjust θ_{off} to the timing when the phase current becomes zero to avoid current conduction in the negative torque section after the negative voltage is applied to the motor. Hence, the output of the PI regulator is set in advance to satisfy the condition mentioned above. The controller in Fig. 6 gives the lower limit to the command value of the zero-phase current because the lower limit value $i_{0min.}$ is used in the design of the damping control in Ref. [9]. The system controls the detected zero-phase current so that it does not fall below $i_{0min.}$ to ensure stability.

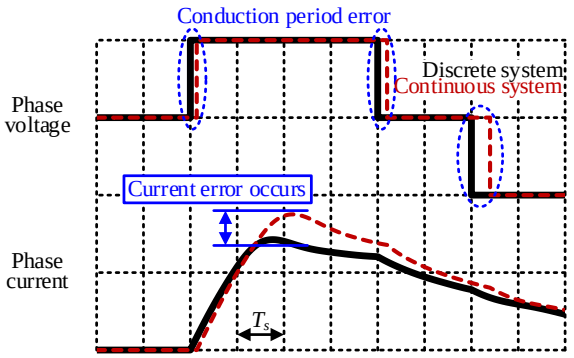

(a) Single-pulse voltage drive without conduction error correction.

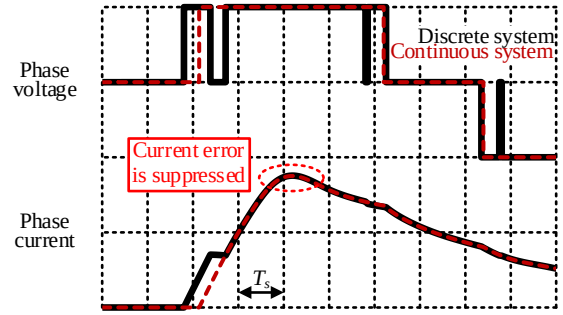

(b) Single-pulse voltage drive with conduction error correction.

Fig. 4. Effect of conduction period error in discrete system.

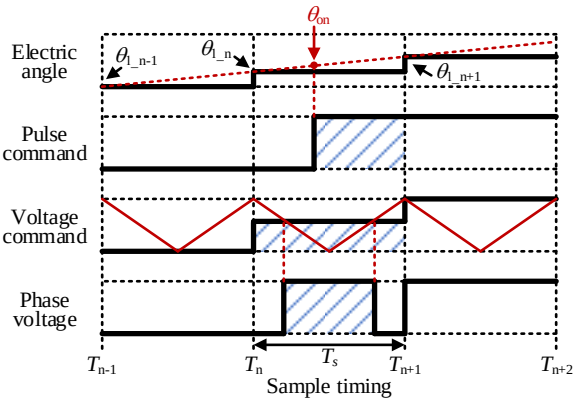

Fig. 5. Voltage command which corrects conduction period error under PWM.

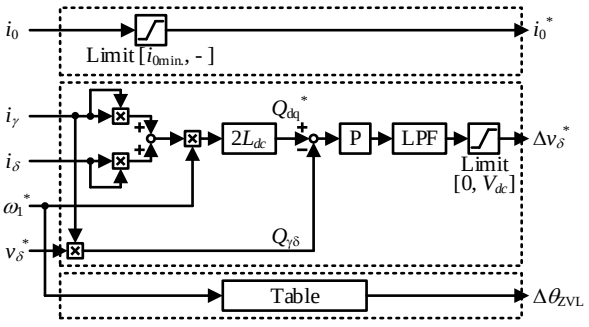

Fig. 6. Block diagram of high-efficiency control.

Next, the i_d=0 control based on the reactive power is explained. In the dq-axis coordinate, the reactive power Q_{dq} under the condition of i_d=0 is expressed as in (7),

$$\begin{aligned} Q_{dq} &= v_q i_d - v_d i_q \\ &= 2\omega\left\{L_{dc}\left(i_d^2 + i_q^2\right)\right\} = 2\omega\left\{L_{dc}\left(i_\gamma^2 + i_\delta^2\right)\right\} \end{aligned} \quad (7),$$

where v_d and v_q are the d-axis and q-axis voltage, respectively, i_d and i_q are the d-axis and q-axis current, respectively, i_γ and i_δ are the γ-axis and δ-axis current, respectively, ω is the electric angular frequency, and L_{dc} is the dc component of the self-inductance. On the other hand, in the γδ-axis coordinate, the reactive power $Q_{\gamma\delta}$ is expressed as in (8),

$$Q_{\gamma\delta} = v_\delta i_\gamma \quad (8)$$

Q_{dq} is independent of i_0. Thus, the v_δ is adjusted by the P regulator to match the reactive power $Q_{\gamma\delta}$ calculated by (8) to the reactive power Q_{dq} calculated by (7) as in Ref. [9].

Table 1 shows the motor parameters, and Fig. 7 shows the loss analysis result when $\Delta\theta_{ZVL}$ changes at the base speed and rated torque. In this paper, the total loss is defined as the mechanical loss, copper loss, and iron loss. The iron loss is identified by subtracting the mechanical output, mechanical loss, and copper loss from the motor input power. In addition, the copper loss is calculated by the winding resistance value that takes temperature characteristics into account. As mentioned in section A, $\Delta\theta_{ZVL}$ in (4) has the degree of freedom in calculating the single pulse voltage.

Fig. 8 shows the i-ϕ characteristics when $\Delta\theta_{ZVL}$ changes. The peak value of the flux linkage is lower when $\Delta\theta_{ZVL}$ is increased. Equation (9) expresses the applied period of the positive voltage to the motor $\Delta\theta_{+V}$ when $\Delta\theta_{ZVL}$ changes,

$$\begin{aligned} \Delta\theta_{+V} &= (\pi - \Delta\theta_{ZVL}/2) - \theta_{on} \\ &= \pi - \Delta\theta_{ZVL}/2 - \arccos\left\{\frac{b_1}{2E_{dc}}\pi - \cos(\Delta\theta_{ZVL}/2)\right\} \end{aligned} \quad (9)$$

In (9), $\Delta\theta_{+V}$ is monotonically decreasing with increasing $\Delta\theta_{ZVL}$. The peak value of the magnetic flux density ΔB is expressed as in (10),

$$\Delta B = \frac{1}{N \cdot A}\int_0^{\Delta\theta_{+V}/\omega_1} E_{dc}\,dt \quad (10),$$

where N is the number of turns of the coil, A is the effective area, and ω_1 is the electric angular frequency. ΔB decreases as $\Delta\theta_{ZVL}$ increases from (9) and (10). Thus, the iron loss decreases since the peak value of the magnetic flux density decreases as the value of $\Delta\theta_{ZVL}$ increases in Fig. 8. On the other hand, the current RMS value (i.e., copper loss) increases with increasing $\Delta\theta_{ZVL}$ due to the longer current conduction period. There is a trade-off relationship between the iron loss and copper loss

Table 1. Motor parameters

Rated power	2.2kW
Base speed(1p.u.), Max. speed	4800rpm, 7200rpm
Max. torque(1p.u.)	4.38Nm
DC voltage	300V
Poles	Stator:18, Rotor:12
Inertia	62.3×10^{-4}kgm^2
Resistance	0.66Ω

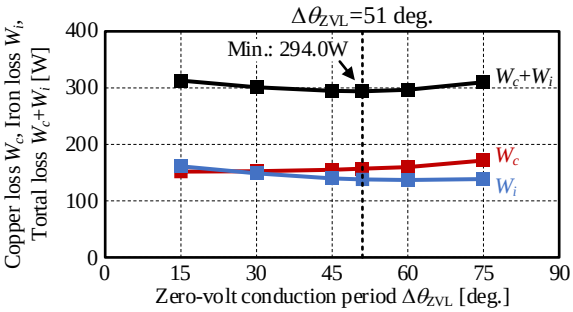

Fig. 7. Loss separation result when $\Delta\theta_{ZVL}$ changes.

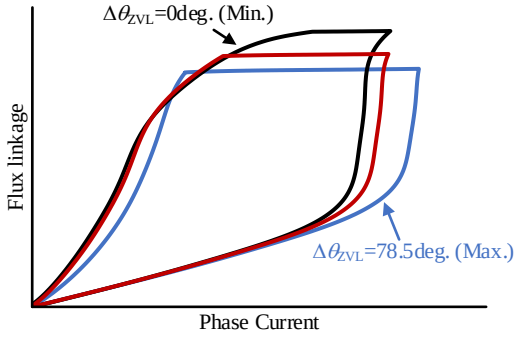

Fig.8. i-ϕ characteristics when $\Delta\theta_{ZVL}$ changes.

concerning $\Delta\theta_{ZVL}$. $\Delta\theta_{ZVL}$ needs to be selected at an appropriate value depending on the operation point to minimize the total loss. In the experiment, the controller refers to the value of $\Delta\theta_{ZVL}$ from the table that minimizes the total loss.

III. Experimental Results

Fig. 9 shows the configuration of the test system. As shown in Fig. 9 (a), the load motor outputs the arbitrary constant torque. In addition, the instantaneous torque is measured by a high-response torque meter (UTMII-10 Nm, 1 kHz bandwidth, UNIPULSE). As shown in Fig. 9 (b), the controller consists of an interface board, 12-bit Analog Digital converter (A/D), Digital Signal Processor (DSP), and Pulse Width Modulation (PWM) module. The greatest part of the control is implemented on the DSP. Exceptionally, only A/D conversion of the detected current and the generation of PWM signal based on voltage command are performed by dedicated parts. The proposed method realizes the single-pulse voltage drive of SRMs without the position sensor using only the DSP.

Fig. 10 shows the drive waveforms at base speed and rated torque. Note that $\Delta\theta_{ZVL}$ in high-efficiency control is set to 51deg. The current RMS value is reduced by 5.8%

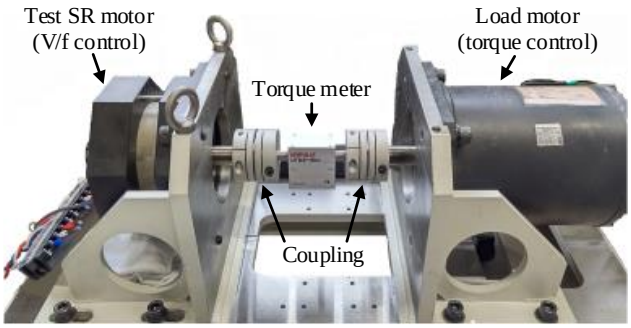

(a) Experimental system.

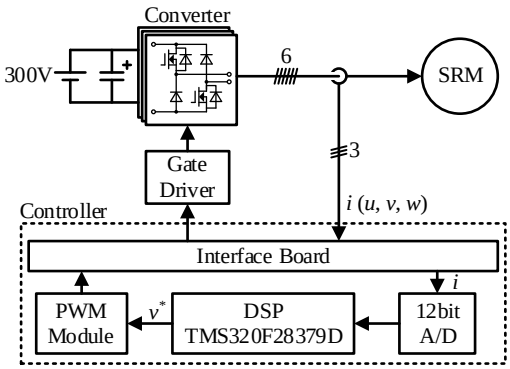

(b) Control system.

Fig. 9. Configuration of test system.

comparing Fig. 10 (c) with (a) because the proposed method reduces the conduction period of motor current in the negative torque section. Fig. 10 (b) shows the result without correction of the conduction period error. A beat occurs in the current peak due to the variation of the switching angle in Fig. 10 (b). On the other hand, the beat is suppressed by the correction method in Fig. 10 (c). Thus, the effect of the correction is verified.

Fig. 11 shows the loss analysis results in Fig. 10 (a) and (c). The proposed single-pulse voltage drive reduces the copper loss by 11.7% and iron loss by 19.2% compared with the conventional sinusoidal voltage drive. The reduction in the iron loss in addition to the copper loss, can be attributed to the reduction in the harmonic iron loss due to the reduction in the number of switching.

Fig. 12 shows the loss analysis results in Fig. 10 (b) and (c). While there is concern about the increase in switching caused by correcting the conduction period error, the copper loss is reduced by 2.4%. This is because the effect of suppressing the peak magnetic flux due to the beat is greater than the increase in the harmonic loss. As shown above, the proposed method reduces the motor drive loss by 14.3% in the experiment. The usefulness of the proposed method is verified.

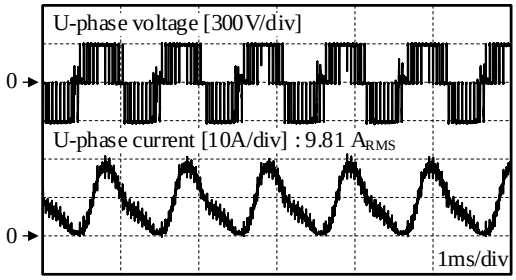

(a) Conventional sinusoidal voltage drive.

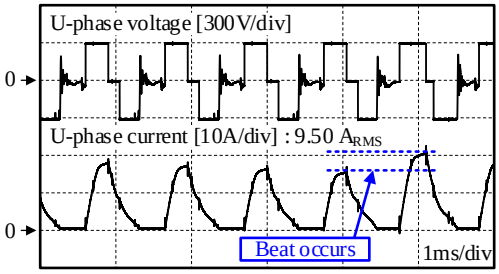

(b) Proposed single-pulse voltage drive without conduction error correction.

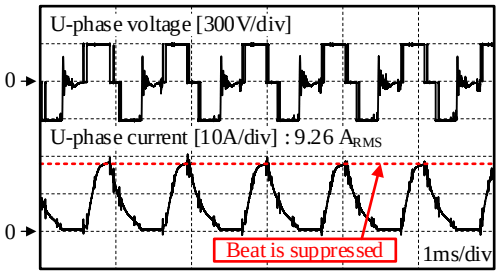

(c) Proposed single-pulse voltage drive with error correction.

Fig. 10. Proposed single pulse voltage drive.

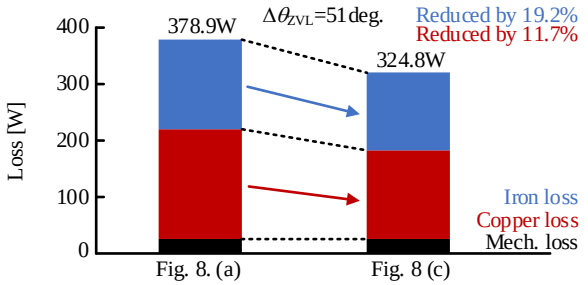

Fig. 11. Loss separation in condition of fig. 10 (a) and (c).

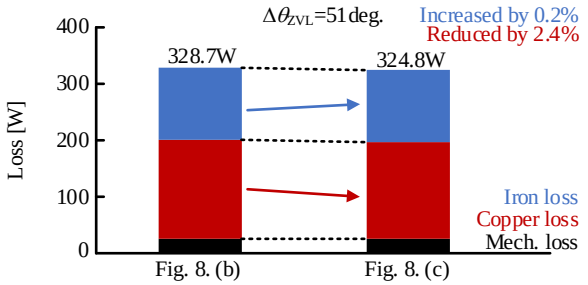

Fig. 12. Loss separation in condition of fig. 10 (b) and (c).

IV. CONCLUSIONS

This paper proposes the single-pulse voltage drive method based on the V/f control of SRMs. The proposed method consists of three parts: (i) generation of the single-pulse voltage, (ii) correction of the conduction period error in the discrete control system, and (iii) high-efficiency control specialized for the single-pulse voltage drive. The experimental results confirm that the proposed method reduces the loss of copper and iron by 11.7% and 19.2%, respectively. The future work will theoretically derive $\Delta\theta_{\mathrm{ZVL}}$ in the high-efficiency control.

REFERENCES

[1] T. Kosaka, A. Kume, H. Wakayama, and N. Matsui, “Development of high torque density and efficiency switched reluctance motor with 0.1 mm short airgap,” 2007 European Conference on Power Electronics and Applications, Aalborg, Denmark, pp.1-9 (2007)

[2] H. Yamai, Y. Sawada, K. Ohyama, “Applying Switched Reluctance Motor to Oil Hydraulic Pump Use,” IEEJ Transactions on Industry Applications, Vol.123, No.2, pp.96-104 (2003)

[3] G. T. Gotz, P. Tillmann, A. V. Hoegen, and R. W. De Doncker, “Stable Equilibrium Rotor Positions for Three-Phase Switched Reluctance Machine,” IEEJ Journal of Industry Applications, Vol.12, No.4, pp.613-623 (2023)

[4] K. -W. Hu, Y. -Y. Chen and C. -M. Liaw, “A Reversible Position Sensorless Controlled Switched-Reluctance Motor Drive With Adaptive and Intuitive Commutation Tunings,” IEEE Transactions on Power Electronics, Vol.30, No.7, pp.3781-3793 (2015)

[5] K. Ha, R. -Y. Kim and R. Ramu, “Position Estimation in Switched Reluctance Motor Drives Using the First Switching Harmonics Through Fourier Series,” IEEE Transactions on Industrial Electronics, Vol.58, No.12, pp.5352-5360 (2011)

[6] G. Gallegos-Lopez, P. C. Kjaer and T. J. E. Miller, “A new sensorless method for switched reluctance motor drives,” IEEE Transactions on Industry Applications, Vol.34, No.4, pp.832-840 (1998)

[7] S. Sumita, K. Deguchi, and Y. Iwaji, “Position Sensorless Control Method for SRM Using Analog Circuit of Type-1 Control System,” IEEJ Transactions on Industry Applications, Vol.137, No.8, pp.612-621 (2017)

[8] Y. Tsujii, S. Morimoto, Y. Inoue, M. Sanada, “Effect of Inductance Model on Sensorless Control Performance of SynRM with Magnetic Saturation,” IEEJ Journal of Industry Applications, Vol.12, No.4, pp.596-602 (2023)

[9] H. Kato, T. Kumagai, J. Itoh, K. Kusaka, and M. Kato, “V/f Control for Switched Reluctance Motor,” IEEJ Journal of Industry Applications, Vol.13, No.3, pp.261-269 (2024)

[10] N. Nakao, K. Akatsu, “Vector Control Specialized for Switched Reluctance Motor Drives,” IEEJ Transactions on Industry Applications, Vol.134, No.12, pp.1006-1015 (2014)

[11] T. Kojima, and R. W. De Doncker, “Impact of Zero-Volt Loop Control on Efficiency of Switched Reluctance Motors,” IEEE Transactions on Industry Applications, Vol.53, No.4, pp.3621-3634 (2017)

[12] W. U. N. Fernando, and M. Barnes, “Electromagnetic Energy Conversion Efficiency Enhancement of Switched Reluctance Motors With Zero-Voltage Loop Current Commutation,” IEEE Transactions on Energy Conversion, Vol.28, No.3, pp.482-492 (2013)

[13] P. Kosmatin, D. Miljavec, and D. Voncina, “Increasing efficiency of the switched reluctance generator at low-speed operation,” 2013 International Conference-Workshop Compatibility And Power Electronics, pp.197-202 (2013)

[14] D. A. Torrey, and J. H. Lang, “Optimal-efficiency excitation of variable-reluctance motor drives,” IEE Proceedings B (Electric Power Applications), Vol.138, No.1, pp.1-14 (1991)

[15] X. D. Xue, K. W. E. Cheng and S. L. Ho, “Online and Offline Rotary Regression Analysis of Torque Estimator for Switched Reluctance Motor Drives,” IEEE Transactions on Energy Conversion, Vol.22, No.4, pp.810-818 (2007)